Colorimetric and fluorescent hydrazone-BODIPY probes for the detection of γ-hydroxybutyric acid (GHB) and cathinones

Silvia Rodríguez-Nuévalos [a], Ana M. Costero [a,b,c], Margarita Parra [a,b,c], Salvador Gil [a,b,c], Pau Arroyo [a,b], Jose A. Sáez [a,b,**], Pablo Gaviña [a,b,c,*], Paola Ceroni [d], Andrea Fermi [d]

[a] *Instituto Interuniversitario de Investigación de Reconocimiento Molecular y Desarrollo Tecnológico (IDM). Universitat Politècnica de València, Universitat de València, Doctor Moliner 50, Burjassot, 46100, Valencia, Spain*
[b] *Departamento de Química Orgánica, Universitat de València, Doctor Moliner 50, Burjassot, 46100, Valencia, Spain*
[c] *CIBER de Bioingeniería, Biometariales y Nanomedicina (CIBER-BBN), Spain*
[d] *Dipartimento di Chimica "G. Ciamician", Università di Bologna, Via Selmi, 2, 40126, Bologna, Italy*

A B S T R A C T

Consumption and abuse of drugs is a general problem, which concerns our entire society. In some cases, drugs are used for recreational purposes; but in others, they are used to commit crimes such as Drug-Facilitated Sexual Assault (DFSA). In other cases, this consumption alters the consumer mood in such a way that risky situations can rise. In any case, detection of drugs in different environment is worthwhile. Here, two new chromogenic and fluorescent probes are reported. Detection of both cathinone derivatives and γ-hydroxybutyric acid (GHB) can be carried out with naked-eye with limits of detection of 0.4 μM and 0.3 μM for GHB and 2.0 μM for ephedrone. Selectivity in the presence of other drugs has been tested. Sensing mechanisms have been studied using different spectroscopic techniques and they have been also corroborated through theoretical calculations.

1. Introduction

Over the last years, the number of drug users in our society has increased alarmingly. According to the statistics from European Monitoring Center for Drugs and Drug Addiction (EMCDDA), around 97 million people aged 15–64 in European Union (EU), almost the third of the population, have consumed illicit drugs at some moment of their lives [1]. Related to this latter issue, it is also considerably worrying the quick emergence of illegal substances known as New Psychoactive Substances (NPS). NPS consist of a noticeably extensive range of uncontrolled and illegal drugs. Not only their consumption has increased in the last three decades, but also their easy replacement for another derivative and their illegal trafficking. In fact, in 2015, 34,000 seizures in EU took place, which implied 4.6 tonnes of seized NPS [2]. In this sense, the importance of synthetic cathinones has risen in the last 10 years.

Synthetic cathinones (SCs), commonly known as "bath salts", are substances chemically related to cathinone (Fig. 1), a stimulant drug found in the khat plant. The synthetic variants of cathinone can be more potent as drugs than the parent natural compound and, in some cases, much more dangerous due to their cardiac and neurological effects.

Some examples of SCs are ephedrone, 3,4-MDPHP (3′,4′-methyl-enedioxy-α-pyrrolidinohexiophenone), MPHP (4′-methyl-α-pyrrolidi-nohexiophenone) and MDMC (3,4-methylenedioxy-*N*-methylcathinone). The qualitative identification of these drugs is usually carried out by the Zimmermann test, which uses 1,3-dinitrobenzene in basic medium to induce a colour change by the formation of a Meisenheimer complex. However, this test is non-specific giving rise to many false positive responses. Therefore, the preparation of more selective sensors to detect these compounds is a hot field in the sensing area [3].

On the other hand, another drug that is generating significantly troublesome situations to law enforcement agencies and authorities is γ-hydroxybutyric acid (GHB or liquid ecstasy). GHB (Fig. 1), a natural product generated during the γ-aminobutyric acid (GABA) metabolism, is involved in the regulation of a high number of neurotransmitters such as GABA, dopamine or 5-hydroxytryptamine. However, this little fatty acid is also an illicit drug whose use has increased considerably. In 2020, GHB was reported as the fifth most consumed drug by Euro-DEN Plus hospitals [4]. This substance was found in 35% of critical care admissions and 11% of drug acute intoxications, highlighting how easy is to
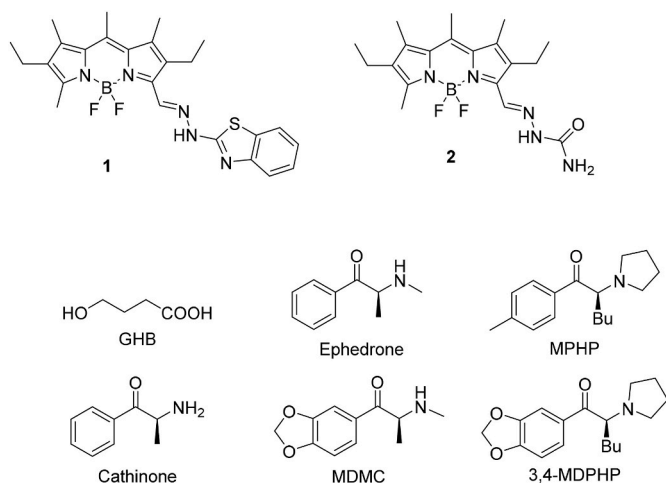

Fig. 1. New prepared probes and structures of selected drugs.

overdose during its consumption. The number of seizures of GHB in Europe also rose to 2000. Furthermore, this compound is implicated in other criminal acts, such as Drug-Facilitated Sexual Assault (DFSA). In that respect, GHB is one of the drugs known as "rape drugs" [5]. Usually, these substances are added to the victims' drinks without their consent, undermining thus their will after ingesting them since they are not able to notice their presence in the drinks. Due to this fact, the number of reports in literature regarding the detection of GHB has increased in the last few years [6,7]. SCs are also likely to be found as "rape drugs" [8].

From this perspective, we focused our effort and attention on the development of chemosensors to detect these drugs: GHB and SCs. In that regard, the use of optical molecular sensors has proved to be very useful, reliable and inexpensive systems for a large number of analytes detection [9,10]. Following our experience in this field [11–13], we now report the preparation and evaluation of two new dyes based on a 4, 4-difluoro-4-bora-3a,4a-diaza-*s*-indacene (borodipyrromethene or BODIPY) moiety functionalized in the alpha position with an hydrazine derivative (Fig. 1). Functionalization has been chosen, on one hand, to explore the acid-base properties of the compounds and their application in GHB detection. On the other hand, the capability of hydrazones to complex Cu(II) salts [14] combined with the well-established redox properties of cathinones, able to reduce Cu(II) to Cu(I), prompted us to study the possibility of using the prepared compounds in combination with Cu(II) to also detect these drugs [15].

2. Material and methods

2.1. Materials

The reagents employed in the synthesis were acquired from Sigma Aldrich and used without further purification. ^{1}H NMR, ^{13}C NMR and ^{19}F NMR spectra were registered with Bruker Avance 300 MHz or 500 MHz spectrometers, all of them referenced to solvent peak, DMSO(d$_6$). All photophysical analyses were carried out in air-equilibrated DMSO or MeCN at 298 K, unless otherwise specified. UV–vis absorption spectra were recorded with a PerkinElmer λ40 or Shimadzu UV-2600 spectrophotometers using quartz cells with path length of 1.0 cm. Luminescence spectra were performed with a PerkinElmer LS-50 or FluoroMax-4 Spectrofluorometer. Lifetimes shorter than 10 μs were measured with an Edinburgh FLS920 spectrofluorometer using time-correlated single-photon counting (TCSPC) technique. Quantum yields were determined with the method of Demas and Crosby [16] using Rhodamine B and Rhodamine 101 as standards (φ$_{fl}$ = 0.7, 0.915, in MeOH and EtOH, respectively). The estimated experimental errors were 2 nm on the band maximum, 5% on the molar absorption coefficient and luminescence

lifetime and 20% on emission quantum yields. Mass spectrometry spectra were carried out with a TripleTOFTM 5600 LC/MS/MS System, with 2 gas sources (both to 35 psi), 450 °C and ion gas voltage of 5500 V. Origin 2020 was the program used to plot titrations and to calculate complexation constants.

2.2. Synthesis of compounds 1 and 2

The synthesis of chemosensors **1** and **2** from BODIPY **3** is summarized in Scheme 1.

2.2.1. Synthesis of 2,6-diethyl-1,3,5,7,8-pentamethyl-4,4-difluoro-4-bora-3a,4a-diaza-s-indacene (3) [17]

2.2 mL (16.30 mmol) of 3-ethyl-2,4-dimethyl-1H-pyrrole were dissolved in 8 mL of dry DCM under inert atmosphere. 3.44 mL (48.38 mmol) of acetyl chloride were added dropwise and the mixture was refluxed for 75 min. Then, the mixure was poured over 40 mL of hexane and solvents were removed under vacuum. The red oil was dissolved in 92 mL of dry DCM under inert atmosphere and 12 mL (86.10 mmol) of NEt$_3$ were added. After stirring 10 min at room temperature, 12 mL (97.23 mmol) of BF$_3$OEt$_2$ were added dropwise and the stirring was kept for 2 h at room temperature. Then, the solvent was removed and the crude was purified by chromatographic column using silical gel as stationary phase and a mixture of hexane:AcOEt 9:1 as eluent. Compound **3** was obtained as an orange solid (1.98 g, 76% yield). ^{1}H NMR (300 MHz, CDCl$_3$) δ 2.60 (s, 3H), 2.49 (s, 3H), 2.40 (q, *J* = 7.6 Hz, 4H), 2.33 (s, 3H), 1.04 (t, *J* = 7.6 Hz, 6H). ^{13}C NMR (126 MHz, CDCl$_3$) δ 151.95, 139.86, 136.47, 132.50, 131.80, 17.26, 17.09, 15.05, 14.52, 12.51.

2.2.2. Synthesis of 2,6-diethyl-1,5,7,8-tetramethyl-4,4-difluoro-4-bora-3a,4a-diaza-s-indacene-3-carbaldehyde (4) [18]

300 mg (0.94 mmol) of compound **3** were dissolved in 8.5 mL of THF and cooled to 0 °C. Then, a solution of 1.074 g (4.71 mmol) of DDQ in 2 mL of THF were added dropwise and, after that, 3.5 mL of THF were added. The mixture was stirred while it was leading to warm slowly to room temperature. The solvent was removed under vacuum and the crude was purified by chromatographic column using silical gel as stationary phase and a mixture of hexane:AcOEt 8:2 as eluent. Compound **4** was isolated as an orange powder (221 mg, 71% yield). ^{1}H NMR (300 MHz, CDCl$_3$) δ 10.34 (t, *J* = 2.1 Hz, 1H), 2.82 (q, *J* = 7.5 Hz, 2H), 2.71 (s, 3H), 2.61 (s, 3H), 2.45 (q, *J* = 7.6 Hz, 2H), 2.40 (s, 3H), 2.34 (s, 3H), 1.09 (m, 6H). ^{13}C NMR (126 MHz, CDCl$_3$) δ 186.01, 163.99, 142.02, 141.91, 138.88, 137.43, 136.93, 132.01, 17.80, 17.62, 17.17, 14.98, 14.63, 14.33, 13.50, 13.16.

2.2.3. Synthesis of compound 1

100 mg (0.30 mmol) of compound **4** were mixed with 65 mg (0.39 mmol) of 2-hydrazinobenzothiazole and 26 mg (0.32 mmol) of sodium acetate in 13 mL of EtOH and refluxed overnight. The solvent was removed under vacuum and the crude was purified by column chromatography on silical gel, using a mixture of hexane/AcOEt 7:3 as eluent. After drying at 40 °C for 1 day, compound **1** was isolated as a dark green powder (99 mg, 68% yield). ^{1}H NMR (500 MHz, DMSO-d$_6$) δ 12.63 (s, 1H), 8.56 (s, 1H), 7.93–7.70 (m, 1H), 7.49 (s, 1H), 7.31 (t, *J* = 7.6 Hz, 1H), 7.13 (t, *J* = 7.6 Hz, 1H), 2.89 (q, *J* = 7.3 Hz, 2H), 2.70 (s, 3H), 2.48 (s, 3H), 2.43 (q, *J* = 7.5 Hz, 2H), 2.38 (s, 3H), 1.18 (t, *J* = 7.3 Hz, 3H), 1.02 (t, *J* = 7.5 Hz, 3H). ^{13}C NMR (126 MHz, DMSO-d$_6$) δ 155.53, 141.20, 139.43, 135.86, 134.10, 133.05, 126.08, 121.94, 121.67, 118.15, 115.50, 17.90, 17.01, 16.41, 14.60, 14.33, 14.23, 13.25, 12.51. ^{19}F NMR (471 MHz, DMSO-d$_6$) δ −137.95, −138.01, −138.09, −138.15. HRMS (ESI$^+$): *m/z* calcd for C$_{25}$H$_{29}$BF$_2$N$_5$S [M+H]$^+$: 480.2210; found: 480.2190. UV–Vis: λ_{max} (DMSO) = 584 nm. Fluorescence emission (DMSO): λ_{max} = 616 nm (λ_{exc} = 500 nm), φ$_{fl}$: 0.39, τ: 2.5 ns.
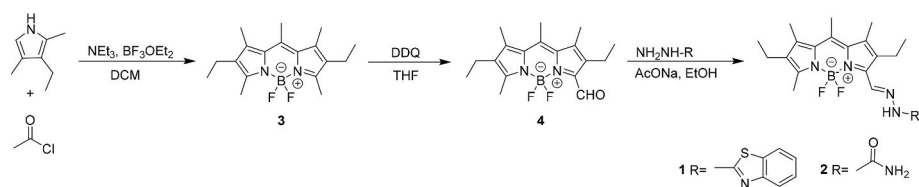
Scheme 1. Synthetic pathway to prepare compounds **1** and **2**.

2.2.4. Synthesis of compound 2

100 mg (0.30 mmol) of compound **4** were mixed with 72 mg (0.65 mmol) of semicarbazide hydrochloride and 79 mg (0.97 mmol) of sodium acetate in 12 mL of EtOH. The mixture was refluxed for 3 h and, after cooling, was filtered under vacuum and dried at 40 °C for 1 day. 104 mg of compound **2** were obtained as a pink solid (83% yield). ^{1}H NMR (500 MHz, DMSO-d_6) δ 10.68 (s, 1H), 8.30 (s, 1H), 2.73 (q, $J = 7.4$ Hz, 2H), 2.69 (s, 3H), 2.45 (s, 3H), 2.41 (q, $J = 7.6$ Hz, 2H), 2.37 (s, 3H), 2.35 (s, 0H), 1.10–0.96 (m, 6H). ^{13}C NMR (126 MHz, DMSO-d_6) δ 156.10, 155.15, 141.44, 141.35, 139.25, 135.92, 133.94, 133.61, 132.82, 132.30, 131.89, 118.15, 115.50, 17.77, 17.01, 16.40, 14.62, 14.21, 14.05, 13.27, 12.46. ^{19}F NMR (471 MHz, DMSO-d_6) δ −138.25, −138.31, −138.39, −138.45. HRMS (ESI⁺): m/z, calcd for $C_{19}H_{27}BF_2N_5O$ [M + H]⁺: 390.2282; found: 390.2268. UV–Vis: λ_{max} (DMSO) = 559 nm. Fluorescence emission (DMSO): λ_{max} = 580 nm (λ_{exc} = 450 nm), φ_{fl}: 0.94, τ: 4.7 ns.

2.3. Sensing experiments

2.3.1. NaGHB detection

In a 3 mL quartz cell (1 cm of path length), 2410 μL of DMSO were mixed with 90 μL of sensor from a 139 μM solution in DMSO. After that, increasing quantities of NaGHB were added from a 1.25 mM solution in DMSO until saturation point was reached.

2.3.2. Interferents measurements (NaGHB)

In a 3 mL quartz cell (1 cm of path length), 90 μL of 139 μM solution of sensor in DMSO were mixed with each interferent (0.3% w/v citric acid, 0.01% w/v sodium ascorbate and 10% sucrose) and diluted until 2500 μL with DMSO.

2.3.3. Real samples (NaGHB)

Initially, drinks were spiked in a 12 mM concentration of NaGHB. Next, an aliquot of 50 μL of each drink was mixed with 50 μL of NaHCO₃ (1 mM in H₂O). 50 μL of this latter mixture were taken and added to a second mixture of 900 μL of DMSO and 50 μL of the sensor (1 mM in DMSO). The whole process was carried out at room temperature and the described changes took place immediately.

2.3.4. Copper complexation

2.3.4.1. Copper(II) titrations. In a 3 mL quartz cell (1 cm of path length), 2410 μL of MeCN were mixed with 90 μL of sensor from a 139 μM solution in MeCN. After that, increasing quantities of Cu(OTf)₂ were added from a 1.25 mM solution in MeCN until saturation point was reached.

2.3.4.2. Copper(I) titrations. In a 3 mL quartz cell (1 cm of path length), 2220 μL of DMSO were mixed with 100 μL of ultra pure water, and 180 μL of sensor from a 139 μM solution in DMSO. After that, increasing quantities of CuBr were added from a 2.5 mM solution in DMSO, with a 3-min period of incubation after each addition, until arriving to saturation point.

2.3.5. Synthetic cathinone titrations

In a 3 mL quartz cell (1 cm of path length), 2220 μL of DMSO were mixed with 100 μL of ultra pure water, 180 μL of sensor from a 139 μM

solution in DMSO and 80 μL of Cu(OTf)₂ from a 1.25 mM solution in DMSO. After that, increasing quantities of ephedrone were added from a 2.5 mM solution in ultra pure water, with a 5-min period of incubation after each addition, until arriving to saturation point.

2.3.6. Interferents measurements (SCs)

In a 3 mL quartz cell (1 cm of path of length), 2220 μL of DMSO were mixed with 100 μL of ultra pure water, 180 μL of sensor from a 139 μM solution in DMSO and 80 μL of Cu(OTf)₂ from a 1.25 mM solution in DMSO. After that, 1 equiv. of ephedrone, NaGHB, SCs or other abuse drugs were added, with a 5-min period of incubation after each addition.

2.3.7. Computational methods

The geometrical optimization of compounds **1** and **2** together with their deprotonated counterparts at the *meso* (**1m** and **2m**) and hydrazone NH positions (**1n** and **2n**) starting from different conformations for their hydrazone side-chain (**-confx**, where x is the conformation number) have been carried out using Gaussian16 rev. A03 program package [19] with the hybrid M062X functional of Truhlar and Zhao [20] using the split-valence triple-ζ 6-311+G(2d,2p) basis set [21–31]. At those conformations of compound **1** where a 1,4-*syn*-periplanar arrangement of nitrogen atoms of its side-chain is able to coordinate Cu(I) cation (**-cu**), the optimization has been carried out using Ahlrichs and co-workers DEF2TZVP basis set [32,33] over the metal center. To take into account the effect of the solvent, DMSO, SMD solvation model was used [34]. Frequency calculations were performed over optimized structures to properly characterize minima structures (no imaginary frequencies).

To explore the electronic transitions responsible for the UV–vis UV–Vis spectra, vertical excitation energies were computed over M062X/6-311+G(2d,2p)/SMD(DMSO) (DEF2TZVP over Cu(I) when present) geometries through single-point TD-DFT [35,36] calculations (15 states, singlets only) in solution using non-equilibrium formalism at the same theory level. From all the TD-DFT calculations submitted, GaussView [37] was used to visualize the results and generate the UV–vis plots using the excitation energies and the oscillator strength for each excited state.

3. Results and discussion

3.1. Synthesis and optical properties of BODIPY-probes

Although there are several methods to synthesize BODIPYs [38], compounds **1** and **2** were synthesized as it is described in Scheme 1. In first place, 3-ethyl-2,4-dimethyl pyrrol was refluxed with acetyl chloride and TFA in DCM. NEt₃ and BF₃OEt₂ were added consecutively and, after purification, derivative **3** was isolated. The synthesis of compound **4** was carried out through a selective oxidation of **3** using DDQ in THF at 0 °C. Finally, derivatives **1** and **2** were synthesized using the appropriate hydrazine derivatives in the presence of AcONa in refluxing EtOH. The structures of compounds **1** and **2** were established by HRMS and ^{1}H, ^{19}F and ^{13}C NMR spectroscopy (see supporting information, Figs. S1–S6).

Once compounds **1** and **2** were obtained, their optical properties were studied in MeCN and DMSO (5 μM both). Derivative **1** showed an absorption band centred at 584 nm and an emission band centred at 616 nm in DMSO (λ_{ex} = 500 nm). In this solvent, compound **1** presented a low intensity absorption band with maximum at 717 nm, most likely

attributed to its deprotonated form. On the other hand, compound **2** exhibited an absorption band centred at 559 nm and an emission profile centred at 580 nm (λ_{ex} = 450 nm). The optical properties of both compounds studied in MeCN showed similar absorption and emission bands and, in any case, no significant solvatochromic effect was observed (see supporting information, Figs. S7–S10). High quantum yields were determined and lifetimes were measured in both solvents. Results obtained in DMSO are summarized in Table 1 (see Table S1 for ones in MeCN), which agree with those found in literature [39].

3.2. Acid-base properties and GHB detection

The acid-base properties of compounds **1** and **2** were evaluated in DMSO solution with different bases: TBAOH, AcONa, DABCO and NEt₃. Neither DABCO nor NEt₃ gave rise to significant modifications in absorption or fluorescence emission (see Fig. S11). On the other hand, strong changes in colour and fluorescence emission were observed for compound **1** with TBAOH and AcONa, while compound **2** showed less intense ones. As can be seen in Fig. S11, the lowest energy absorption band, corresponding to the BODIPY core, disappeared after the addition of 1 equiv. of TBAOH in the case of compound **1** and decreased significantly for compound **2**, being the effect on **1** stronger than in **2**. In addition to this effect, in the case of compound **1** the absorption band peaked at 717 nm increased in intensity, whilst for compound **2** a new band appeared at lower wavelength (355 nm). A strong quenching of fluorescence was observed for both probes upon the base addition (see Fig. S12).

These results indicated that whereas the anion generated from compound **1** led to an enhancement of the conjugation of the BODIPY core, resulting in a bathochromic shift of the main absorption band, that originated from compound **2** disrupted this conjugation, since an hypsochromic effect was observed. This opposite behaviour suggested that **1** underwent a deprotonation at the hydrazone NH, giving rise to an increase in the electronic delocalization of the molecule, whereas **2** was deprotonated at the methyl group at the *meso* position of the BODIPY (Fig. 2), thereby justifying the loss of conjugation.

This hypothesis was tested using both experimental and theoretical data. Thus, NMR spectra were registered for both probes with and without the presence of 1 equiv. of TBAOH. When the base is placed with compound **2**, several changes were observed in both ¹H and ¹³C NMR spectra: (a) only three signals (2.20, 2.13 and 2.10 ppm) of the methyl groups directly bond to the BODIPY core appeared instead of the four signals of the initial compound, (b) a couple of peaks at 5.05 ppm corresponding to two olefinic hydrogens appeared and (c) a signal around 101 ppm in the ¹³C NMR spectrum corresponding to an olefinic carbon appeared (see Fig. 3 and S13), which clearly accords with the anion structure proposed in Fig. 2.

By contrast, in the case of compound **1**, the greatest portion of deprotonation took place at the NH of the hydrazone group since the signal around 12.66 ppm in the ¹H NMR spectrum disappeared completely. At the same time, a small portion of compound **1** was also deprotonated at the *meso* position as a pair of peaks around 5.10 ppm were observed (see Fig. S14).

To confirm these results, the acid-base properties of compounds **1** and **2** were studied through theoretical calculations, computing the pK$_a$ of selected positions in both molecules in DMSO. Whereas in compound **2** the H in *meso* position was, by far, the most acidic one; in compound **1** there were two H with similar calculated acidity (Fig. 4). The slightly

most acidic one was the H from the NH of the hydrazone group, which was in agreement with NMR experiments and UV–vis spectra since the largest deprotonation in that position has been demonstrated by the complete disappearance of the NH peak in the ¹H NMR spectrum and the bathochromic shift of the main band observed in UV–vis spectra. Experimental maximum absorption bands shifts were compared to theoretical ones (see Table S2).

Next, the utility of the new probes in detecting NaGHB was explored. To do that, absorption and emission titrations using both compounds were carried out (see Fig. 5 for absorption changes and Fig. S15 for emission ones). As can be observed in Fig. 5A, addition of increasing amounts of NaGHB to a 5 μM DMSO solution of compound **1** induced a linear decrease of the absorption band at 584 nm with a concomitant increase in the band at 717 nm. The increase of this band is responsible for the colour change observed in the solution (from purple to green). In the case of compound **2**, the decrease of the band at 559 nm was observed with the simultaneous increase of the band at 355 nm, with its corresponding colour disappearance.

From the titration experiments carried out, the limits of detection (LoD) could be determined, using the expression: $LoD = \frac{3 \cdot S_b}{m}$, where S_b is the blank standard deviation and m the slope. The values obtained were 0.4 μM for compound **1** and 0.3 μM for compound **2**. Since these probes may be potentially able to detect GHB in real samples, it is worth noticing that these values are considerably lower than the amount of GHB necessary to induce severe effects (50 mg kg^{-1}), which is around 75 mM (assuming an average weight of 62 kg in a standard volume of 330 mL) [40].

Aiming at exploring the possible usability of the sensor in beverages, several interferents present in these media (citric acid, sodium ascorbate and sucrose at their usual concentration in drinks) were analysed in presence and absence of NaGHB (see Fig. S16 for absorption changes for compounds **1** and **2** and Fig. S17 for fluorescence changes). No significant absorption changes were observed in any case, after the addition of the interferents, and both compounds were still capable of detecting NaGHB in a much lower concentration than that usually used in a recreational environment [40].

With these promising results in mind, we decided to test compounds **1** and **2** in real samples, in order to ensure their use to detect GHB in drinks. For this reason, some soft drinks were spiked with NaGHB (12 mM). An aliquot of each one was slightly neutralised with NaHCO₃ and mixed with the sensor (100 μM in DMSO). The changes in the emission intensity were immediately observed at room temperature under a common UV lamp. Results for compound **1** are shown in Fig. 6. Those for compound **2** are summarized in supporting information (Fig. S18).

3.3. Copper complexation and synthetic cathinone detection

Going a step further, the utility of the new probes in detecting SCs was explored. First, studies of Cu(II) and Cu(I) complexation with ligands **1** and **2** in different solvents were carried out (see Figs. S19–S20 in supporting information for the studies carried out in MeCN). These studies showed that whereas compound **2** did not exhibit any interaction with either Cu(II) or Cu(I) in DMSO, compound **1** showed different behavior depending on the cation. Thus, Cu(II) gave rise to little changes, especially in absorbance, whereas Cu(I) induced notable changes in both the absorption and the emission spectra of compound **1** (see Fig. S21). A bathochromic shift of the absorption band from 584 nm to 632 nm as well as a fluorescence emission quenching was observed for **1** in the presence of an excess of Cu(I) (Fig. 7). This different behaviour could be used to detect cathinones since it has been described in the literature that these compounds are suitable reducing agents for Cu(II) [15]. In a first stage, complexation of compound **1** with Cu(I) was carefully studied. Thus, we carried out titration experiments with increasing amounts of Cu(I), observing the formation of a 1:1 complex, whose association constant was determined as 9.22·10⁴ M^{-1} [41]. The

Table 1

Absorption and emission maximums, quantum yields and lifetimes of compounds **1** and **2** in DMSO.

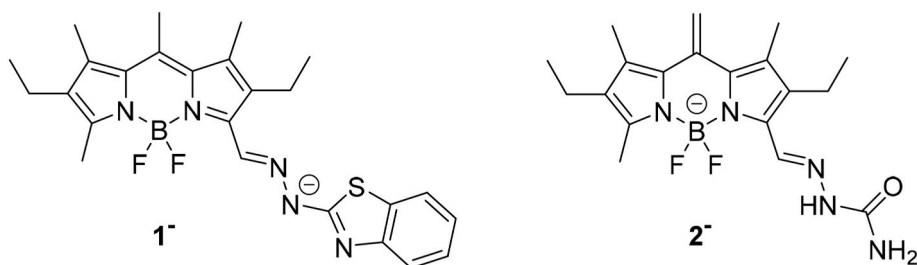| COMPOUND	λ_{abs} (nm)	λ_{em} (nm)	φ	τ (ns)
1	584	616	0.39	2.5
2	559	580	0.94	4.7

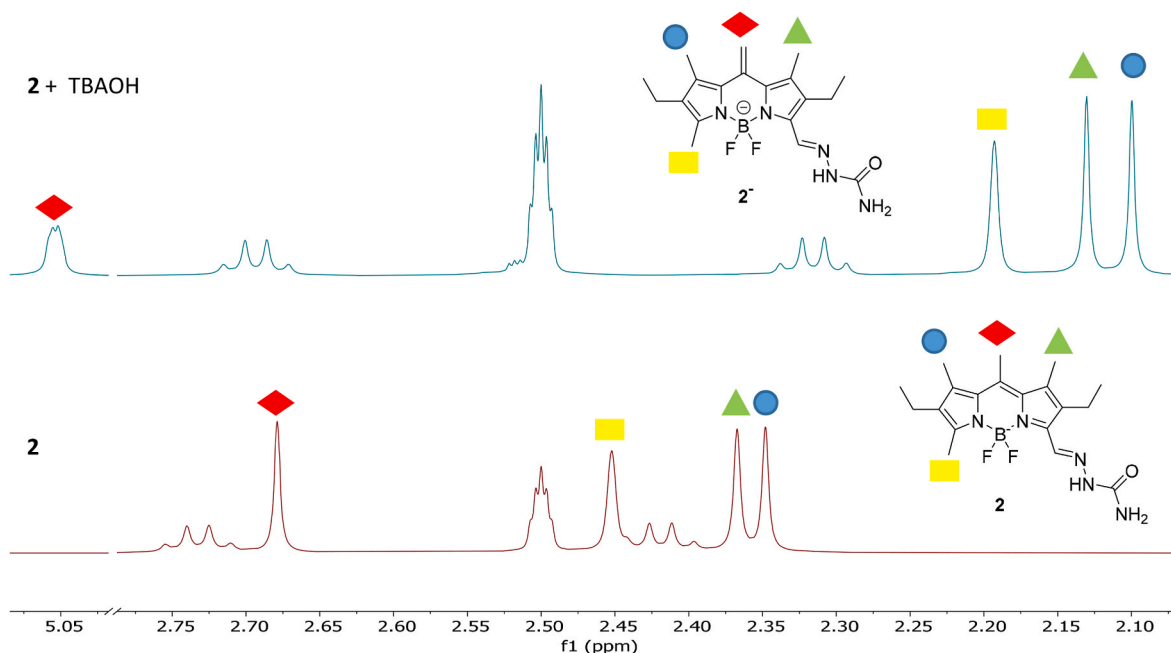**Fig. 2.** Proposed anions generated by probes **1** and **2** in presence of TBAOH.

Fig. 3. Changes observed in ^{1}H NMR spectra of compound **2** (DMSO-d_6) upon the addition of 1 equiv. of TBAOH (showed from 5.10 to 2.05 ppm).
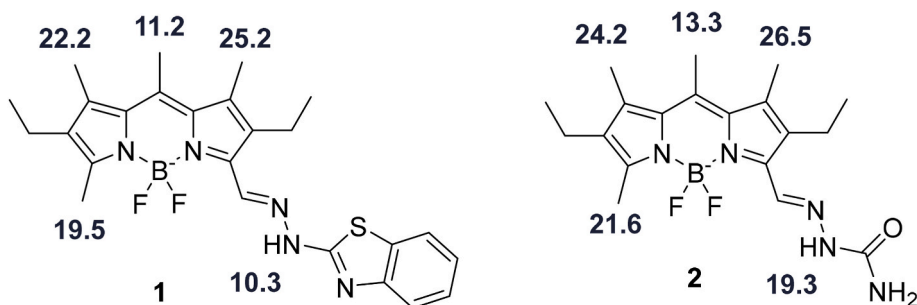

Fig. 4. Calculated pK$_a$ of selected positions at each BODIPY-derivative in DMSO.

starting point of the titration (black line) showed a less intense absorption of the band centred at 717 nm most likely due to the presence of some water.

Since different results were obtained during the complexation studies of Cu(II) and Cu(I) in DMSO, we decided to explore the detection of ephedrone through the reduction of a salt of Cu(II) in the presence of probe **1**. To do so, sensing conditions were optimized and the measurements were carried out using 10 μM of compound **1**, 4 equiv. of Cu (OTf)$_2$, a mixture of DMSO:H$_2$O 96:4 as solvent and an incubation period of 5 min.

As can be observed in Fig. 8, the addition of increasing amounts of ephedrone to a mixture of compound **1** and Cu(II) resulted in a progressive fluorescence emission quenching of **1**. From the titration results (Fig. 8B), a LoD of 2.0 μM was found (see Fig. S22 for absorption titration results). Since a potential application of this probe could be the identification of SCs in seized materials, the visual observation of the fluorescence quenching under a simple and portable UV-lamp would allow the enforcement officers in few minutes to discover whether or not those substances are SCs.

To verify whether the mixture of compound **1** and Cu(II) was a useful sensor for the detection of other cathinones, the behaviour of several SCs such as: 3,4-MDPHP MPHP and MDMC was studied under the previous experimental conditions. Emission changes are shown in Fig. 9 (see Fig. S23 for absorption changes).
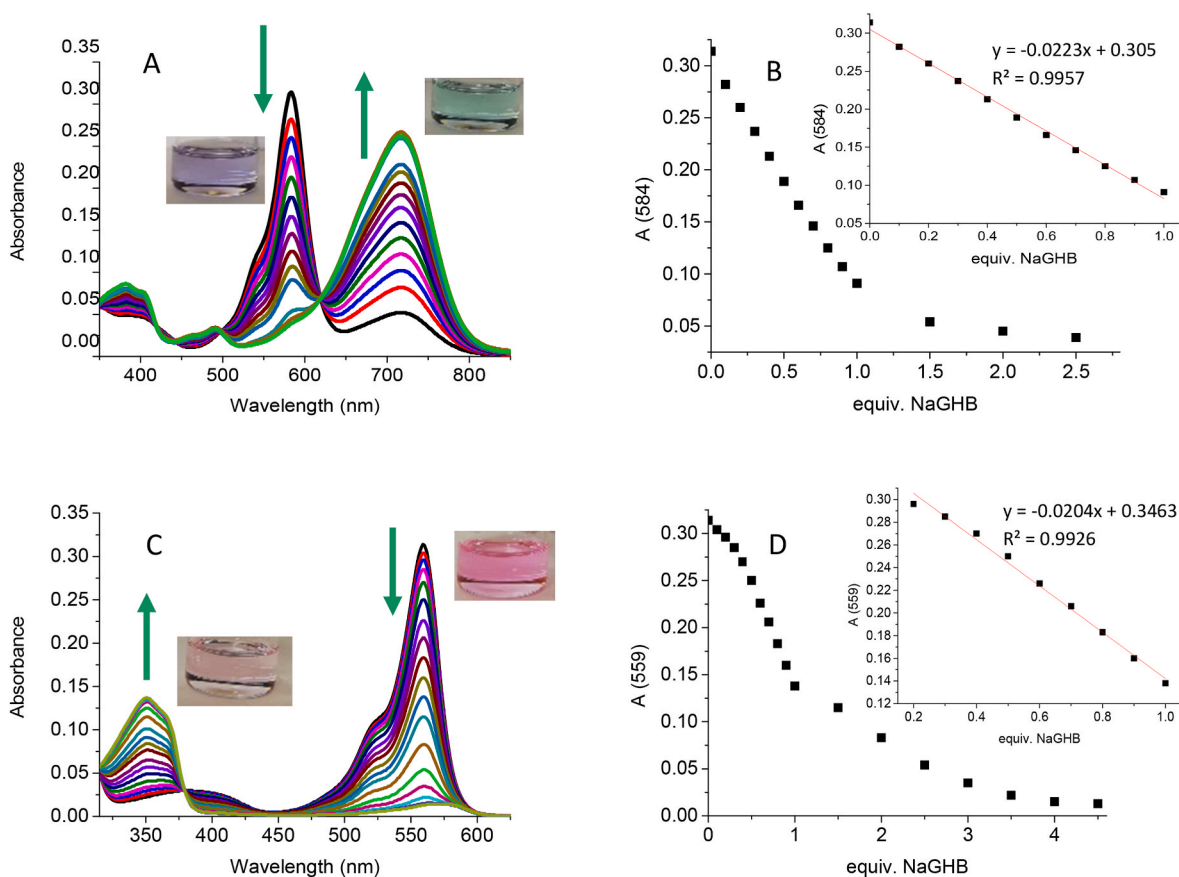
Fig. 5. A) Absorption changes observed in probe **1** (5 μM in DMSO) with increasing amounts of NaGHB (0–2.5 equiv.). B) Changes in absorbance at 584 nm of probe **1** upon the addition of increasing amounts of NaGHB and its linear regression. C) UV–Visible spectra changes observed for compound **2** (5 μM in DMSO) with increasing amounts of NaGHB (0–4.5 equiv.). D) Absorption changes at 559 nm of compound **2** upon the addition of increasing amounts of NaGHB and its linear regression.
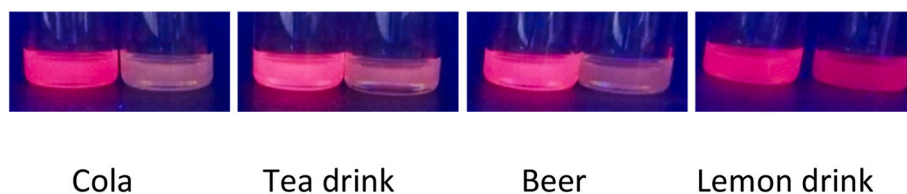

Cola   Tea drink   Beer   Lemon drink

Fig. 6. Changes in emission of probe **1** in the presence of NaGHB in soft drinks. Notice that left vial means non-spiked drink, whilst the right vial stands for the spiked ones.
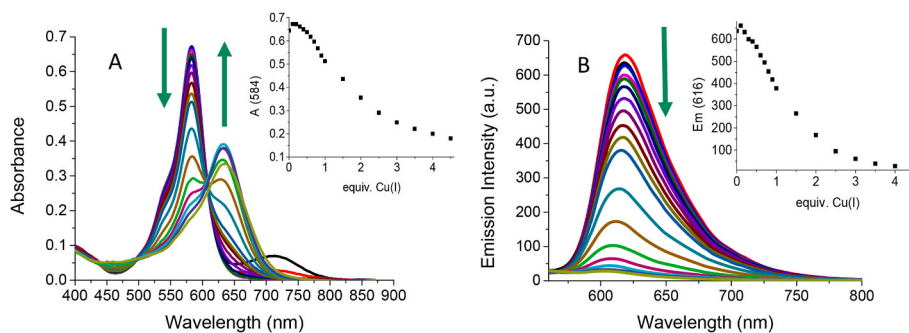

Fig. 7. A) Absorption and (B) emission (λ_{ex} = 500 nm) changes observed for compound **1** (10 μM in DMSO:H_2O 96:4) after the addition of increasing quantities of CuBr (0–4.5 equiv.) and their reaction profiles at 584 nm and 616 nm, respectively (insets).
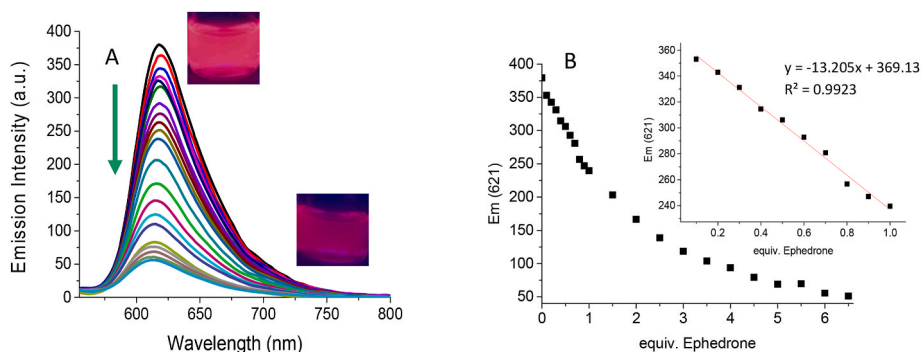
Fig. 8. A) Emission changes observed for probe **1** (10 μM in DMSO:H$_2$O 96:4, 4 equiv. of Cu(OTf)$_2$, λ_{ex} = 500 nm) with increasing quantities of ephedrone (0–6.5 equiv.). B) Changes in fluorescence for probe **1** (10 μM in DMSO:H$_2$O 96:4, 4 equiv. of Cu(OTf)$_2$, λ_{ex} = 500 nm) upon the addition of increasing amounts of ephedrone (0–6.5 equiv.).
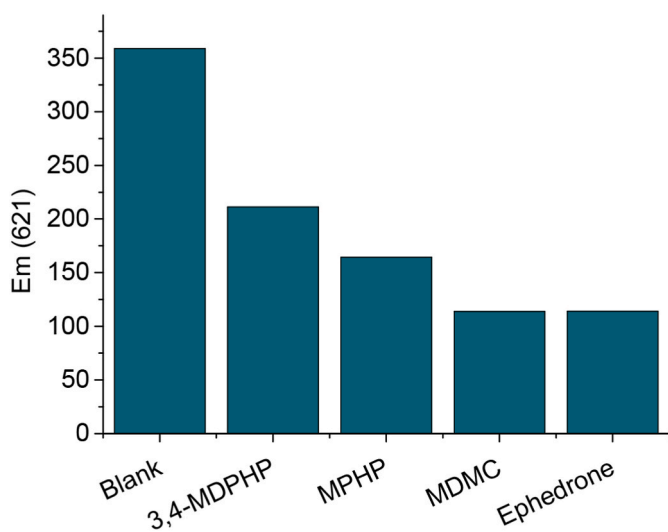

Fig. 9. Emission changes for probe **1** at 621 nm (10 μM in DMSO:H$_2$O 96:4, 4 equiv. of Cu(OTf)$_2$, λ_{ex} = 500 nm) upon the addition of 2 equiv. of SCs.

Fig. 10. Fluorescence spectra changes of probe **1** at 621 nm (10 μM in DMSO: H$_2$O 96:4, 4 equiv. of Cu(OTf)$_2$, λ_{ex} = 500 nm) upon the addition of 1 equiv. other abuse drugs.

As can be seen, the response promoted by the presence of 2 equiv. of ephedrone is similar to the rest of SCs, highlighting the potential application of compound **1** to detect any SCs. It is also noteworthy that, regardless of the type of substitution present in cathinone core as well as the type of amine (primary, secondary or tertiary) they present, these SCs are able to reduce Cu(II) to Cu(I) and the subsequent Cu(I) formed can be detected by probe **1**.

As compound **1** was able to recognize separately GHB and cathinone, we tried to detect GHB using the new established conditions, i.e. in the presence of Cu(II) and a mixture of 96:4 of DMSO:H$_2$O. Satisfactory results were obtained since compound **1** demonstrated that was capable not only of detecting NaGHB alone, but also when both drugs were simultaneously present (absorption and emission changes are summarized in Fig. S24). These results highlighted that the presence of Cu(II) did not affect the NaGHB detection and extends the scope of the prepared sensor.

Finally, other abuse drugs such as benzodiazepines, scopolamine and ketamine were tested as potential interferents (Fig. 10 and S25). No remarkable changes were observed in the presence of any of them. Only the mixture of NaGHB and ephedrone gave rise to a significant response, even in the presence of the other drugs.

4. Conclusions

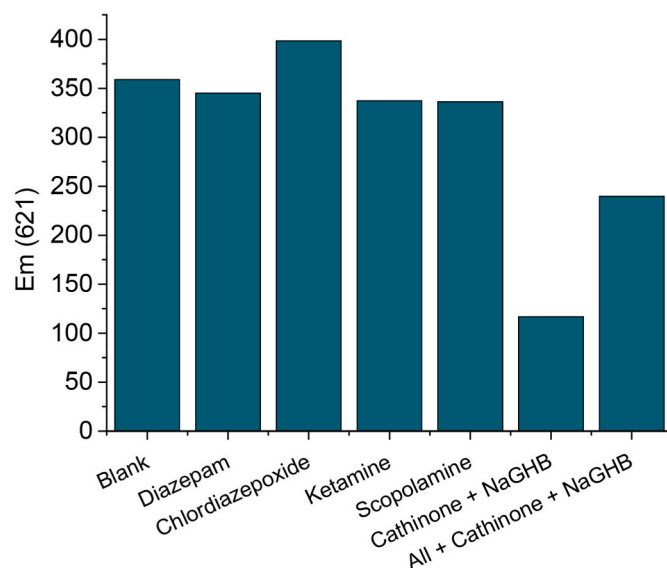Two novel compounds (**1** and **2**) based on a BODIPY-hydrazone core

have been prepared and their photophysical properties studied in two different solvents: DMSO and MeCN. The acid-base properties of both compounds were evaluated by spectroscopic techniques and the observed results corroborated by theoretical calculations. These probes can be used to detect NaGHB through an acid-base reaction. In presence of this drug, both probes showed a significant quenching fluorescence that can be easily observed under a laboratory UV lamp or with the typical light in pubs or discos and a change of colour that can be appreciated with naked-eye. The LoD determined were 0.4 μM for compound **1** and 0.3 μM for compound **2**, making them suitable to point out the presence of GHB in spiked drinks. Additionally, the different complexation behaviour of compound **1** toward Cu(I) and Cu(II) salts in DMSO makes it suitable to detect SCs. The sensing mechanism in this case is based on the capability of cathinones to reduce Cu(II) to Cu(I). The limit of detection determined was 2.0 μM. In this case, the detection of SCs could be focused on the identification of seized materials, since the quenching of the fluorescence is readily noticed using a laboratory UV lamp. Finally, the mixture of **1** and Cu(II) is also capable to detect SCs and NaGHB simultaneously.

CRediT authorship contribution statement

Silvia Rodríguez-Nuévalos: Methodology, Writing – original draft,

Writing – review & editing. **Ana M. Costero:** Conceptualization, Funding acquisition. **Margarita Parra:** Methodology, Writing – original draft. **Salvador Gil:** Methodology, Writing – original draft, All authors have read and agreed to the published version of the manuscript. **Pau Arroyo:** Data curation. **Jose A. Sáez:** Data curation, Writing – review & editing, Supervision. **Pablo Gaviña:** Conceptualization, Funding acquisition, Writing – review & editing, Supervision. **Paola Ceroni:** Data curation. **Andrea Fermi:** Data curation.

Declaration of competing interest

The authors declare that they have no known competing financial interests or personal relationships that could have appeared to influence the work reported in this paper.

Data availability

No data was used for the research described in the article.

Appendix A. Supplementary data

Supplementary data to this article can be found online at https://doi.org/10.1016/j.dyepig.2022.110757.

References

[1] OECD/European Union. Illicit drug consumption among adults. In: Health at a glance: Europe 2020: state of Health in the EU cycle. Paris: OECD Publishing; 2020. https://doi.org/10.1787/fc8a3fcf-en.

[2] European Monitoring Centre for Drugs and Drug Addiction. New psychoactive substances: 25 years of early warning and response in Europe. An update from the EU Early Warning System (June 2022). Luxembourg: Publications Office of the European Union; 2022.

[3] Shafi A, Berry AJ, Sumnall H, Wood DM, Tracy DK. New psychoactive substances: a review and updates. Ther. Adv. Psychopharmacol. 2020;10:1–21. https://doi.org/10.1177/2045125320967197.

[4] European Monitoring Centre for Drugs and Drug Addiction. European drug report 2022: trends and developments. Luxembourg: Publications Office of the European Union; 2022.

[5] Busardò FP, Varì MR, di Trana A, Malaca S, Carlier J, di Luca NM. Drug-facilitated sexual assaults (DFSA): a serious underestimated issue. Eur Rev Med Pharmacol Sci 2019;23:10577–87. https://doi.org/10.26355/eurrev_201912_19753.

[6] 4 (a) Wang W, Dong Z-Z, Yang G, Leung C-H, Lin S, Ma D-L. A long-lived iridium (III) chemosensor for the real-time detection of GHB. J Math Chem B 2017;5:2739–42. https://doi.org/10.1039/C6TB03396B.

[7] Bennett MJ, Steiner RR. Detection of gamma-hydroxybutyric acid in various drink matrices via AccuTOF-DART. J Forensic Sci 2009;54:370–5. https://doi.org/10.1111/j.1556-4029.2008.00955.x.

[8] Hagan KS, Reidy L. Detection of synthetic cathinones in victims of sexual assault. Forensic Sci Int 2015;257:71–5. https://doi.org/10.1016/j.forsciint.2015.07.040.

[9] Anzar N, Suleman S, Parvez S, Narang J. A review on Illicit drugs and biosensing advances for its rapid detection. Process Biochem 2022;113:113–24. https://doi.org/10.1016/j.procbio.2021.12.021.

[10] Costero AM, Parra M, Gil S, Gaviña P. BODIPY core as signaling unit in chemosensor design. In: Bañuelos-Prieto J, Sola Llano R, editors. BODIPY dyes - a privilege molecular scaffold with tunable properties. IntechOpen (London); 2019. https://doi.org/10.5772/intechopen.75220. chaper 2.

[11] Rodríguez-Nuévalos S, Parra M, Gil S, Gaviña P, Arroyo P, Sáez JA, Costero AM. Heteroditopic chemosensor for detecting γ-hydroxybutyric acid (GHB) in soft drinks and alcoholic beverages. Analyst 2022;146:5601–9. https://doi.org/10.1039/D1AN01084K.

[12] Rodríguez-Nuévalos S, Costero AM, Gil S, Parra M, Gaviña P. Bifunctionalized gold nanoparticles for the colorimetric detection of the drug γ-hydroxybutyric acid (GHB) in beverages. Chemosensors 2021;9:160. https://doi.org/10.3390/chemosensors9070160.

[13] Rodríguez-Nuévalos S, Costero AM, Arroyo P, Sáez JA, Parra M, F- Sancenón, Martínez-Máñez R. Protection against chemical submission: naked-eye detection of γ-hydroxybutyric acid (GHB) in soft drinks and alcoholic beverages. Chem Commun 2020;56:12600–3. https://doi.org/10.1039/D0CC05387B.

[14] Vrdoljak V, Pavlovic G, Maltar-Strmeckic N, Cindric M. Copper(II) hydrazone complexes with different nuclearities and geometries: synthetic methods and ligand substituent effects. New J Chem 2016;40:9263–74. https://doi.org/10.1039/C6NJ01036A.

[15] Philp M, Shimmon R, Tahtouh M, Fu S. Development and validation of a presumptive color spot test method for the detection of synthetic cathinones in seized illicit materials. Forensic Chem 2016;1:39–50. https://doi.org/10.1016/j.forc.2016.06.001.

[16] Crosby GA, Demas JN. Measurement of photoluminescence quantum yields. Review, J. Phys. Chem. 1971;75:991–1024. https://doi.org/10.1021/j100678a001.

[17] Yang L, Simionescu R, Lough A, Yan H. Some observations relating to the stability of the BODIPY fluorophore under acidic and basic conditions. Dyes Pigments 2017;46:264–7. https://doi.org/10.1016/j.dyepig.2011.03.027.

[18] Zhang X-F. BisBODIPY as PCT-based halogen free photosensitizers for highly efficient excited triplet state and singlet oxygen formation: tuning the efficiency by different linking positions. Dyes Pigments 2017;146:491–501. https://doi.org/10.1016/j.dyepig.2017.07.051.

[19] Gaussian 16, Revision 03 A, Frisch MJ, Trucks GW, Schlegel HB, Scuseria GE, Robb MA, Cheeseman JR, Scalmani G, Barone V, Petersson GA, Nakatsuji H, Li X, Caricato M, Marenich AV, Bloino J, Janesko BG, Gomperts R, Mennucci B, Hratchian HP, Ortiz JV, Izmaylov AF, Sonnenberg JL, Williams-Young D, Ding F, Lipparini F, Egidi F, Goings J, Peng B, Petrone A, Henderson T, Ranasinghe D, Zakrzewski VG, Gao J, Rega N, Zheng G, Liang W, Hada M, Ehara M, Toyota K, Fukuda R, Hasegawa J, Ishida M, Nakajima T, Honda Y, Kitao O, Nakai H, Vreven T, Throssell K, Montgomery Jr JA, Peralta JE, Ogliaro F, Bearpark MJ, Heyd JJ, Brothers EN, Kudin KN, Staroverov VN, Keith TA, Kobayashi R, Normand J, Raghavachari K, Rendell AP, Burant JC, Iyengar SS, Tomasi J, Cossi M, Millam JM, Klene M, Adamo C, Cammi R, Ochterski JW, Martin RL, Morokuma K, Farkas O, Foresman JB, Fox DJ. Wallingford CT: Gaussian, Inc.; 2016.

[20] Zhao Y, Truhlar DG. The M06 suite of density functionals for main group thermochemistry, thermochemical kinetics, noncovalent interactions, excited states, and transition elements: two new functionals and systematic testing of four M06-class functionals and 12 other functionals. Theor Chem Acc 2008;120:215–41. https://doi.org/10.1007/s00214-007-0310-x.

[21] Petersson GA, Bennett A, Tensfeldt TG, Al-Laham MA, Shirley WA, Mantzaris J. A complete basis set model chemistry. I. The total energies of closed-shell atoms and hydrides of the first-row atoms. J Chem Phys 1988;89:2193–218. https://doi.org/10.1063/1.455064.

[22] Petersson GA, Al-Laham MA. A complete basis set model chemistry. II. Open-shell systems and the total energies of the first-row atoms. J Chem Phys 1991;94:6081–90. https://doi.org/10.1063/1.460447.

[23] McLean AD, Chandler GS. Contracted Gaussian-basis sets for molecular calculations. I. Second row atoms, Z=11-18. J Chem Phys 1980;72:5639–48. https://doi.org/10.1063/1.438980.

[24] Raghavachari K, Binkley JS, Seeger R, Pople JA. Self-consistent molecular orbital methods. 20. Basis set for correlated wave-functions. J Chem Phys 1980;72:650–4. https://doi.org/10.1063/1.438955.

[25] Blaudeau P, McGrath MP, Curtiss LA, Radom L. Extension of Gaussian-2 (G2) theory to molecules containing third-row atoms K and Ca. J Chem Phys 1997;107:5016–21. https://doi.org/10.1063/1.474865.

[26] Wachters AJH. Gaussian basis set for molecular wavefunctions containing third-row atoms. J Chem Phys 1970;52:1033. https://doi.org/10.1063/1.1673095.

[27] Hay PJ. Gaussian basis sets for molecular calculations – representation of 3D orbitals in transition-metal atoms. J Chem Phys 1977;66:4377–84. https://doi.org/10.1063/1.433731.

[28] Raghavachari K, Trucks GW. Highly correlated systems: excitation energies of first row transition metals Sc-Cu. J Chem Phys 1989;91:1062–5. https://doi.org/10.1063/1.457230.

[29] Binning Jr RC, Curtiss LA. Compact contracted basis-sets for 3rd-row atoms – GA-KR. J Comput Chem 1990;11:1206–16. https://doi.org/10.1002/jcc.540111013.

[30] McGrath MP, Radom L. Extension of Gaussian-1 (G1) theory to bromine-containing molecules. J Chem Phys 1991;94:511–6. https://doi.org/10.1063/1.460367.

[31] Curtiss LA, McGrath MP, Blaudeau J-P, Davis NE, Binning Jr RC, Radom L. Extension of Gaussian-2 theory to molecules containing third-row atoms Ga-Kr. J Chem Phys 1995;103:6104–13. https://doi.org/10.1063/1.470438.

[32] Weigend F, Ahlrichs R. Balanced basis sets of split valence, triple zeta valence and quadruple zeta valence quality for H to Rn: design and assessment of accuracy. Phys Chem Chem Phys 2005;7:3297–305. https://doi.org/10.1039/B508541A.

[33] Weigend F. Accurate Coulomb-fitting basis sets for H to Rn. Phys Chem Chem Phys 2006;8:1057–65. https://doi.org/10.1039/B515623H.

[34] Marenich AV, Cramer CJ, Truhlar DG. Universal solvation model based on solute electron density and a continuum model of the solvent defined by the bulk dielectric constant and atomic surface tensions. J Phys Chem B 2009;113:6378–96. https://doi.org/10.1021/jp810292n.

[35] Adamo C, Jacquemin D. The calculations of excited-state properties with time-dependent density functional theory. Chem Soc Rev 2013;42:845–56. https://doi.org/10.1039/C2CS35394F.

[36] Laurent AD, Adamo C, Jacquemin D. Dye chemistry with time-dependent density functional theory. Phys Chem Chem Phys 2014;16:14334–56. https://doi.org/10.1039/C3CP55336A.

[37] GaussView Version 5, Roy Dennington, Keith Todd, Millam John. Shawnee Mission, KS: Semichem Inc.; 2009.

[38] Boens N, Verbelen B, Ortiz MJ, Jiao L, Dehaen W. Synthesis of BODIPY dyes through postfunctionalization of the boron dipyrromethene core. Coord Chem Rev 2019;399:213024. https://doi.org/10.1016/j.ccr.2019.213024.

[39] Bañuelos J. BODIPY dye the most versatile fluorophore ever? Chem Rec 2016;16:335–48. https://doi.org/10.1002/tcr.201500238.

[40] Huller C, Thai D, Jacob III P, Dyer JE. GHB urine concentrations after single-dose administration in humans. J Anal Toxicol 2006;30:360–4. https://doi.org/10.1093/jat/30.6.360.

[41] Diaz de Greñu B. Detection and discrimination of organic contaminants and metabolites of high environmental impact by means of fluorogenic probes. PhD Thesis. Spain): University of Burgos; 2014.